INL/JOU-17-42937-Revision-0

The AGR-3/4 Fission Product Transport Irradiation Experiment

Blaise Collin, Grant L. Hawkes, Joe Palmer, Binh Pham, Dawn Scates, James Sterbentz, Paul A Demkowicz, David A Petti

February 2018

The INL is a U.S. Department of Energy National Laboratory
operated by Battelle Energy Alliance

INL/JOU-17-42937-Revision-0

The AGR-3/4 Fission Product Transport Irradiation Experiment

Blaise Collin, Grant L. Hawkes, Joe Palmer, Binh Pham, Dawn Scates, James Sterbentz, Paul A Demkowicz, David A Petti

February 2018

Idaho National Laboratory
Idaho Falls, Idaho 83415

http://www.inl.gov

Prepared for the
U.S. Department of Energy

Under DOE Idaho Operations Office
Contract DE-AC07-05ID14517

The AGR-3/4 Fission Product Transport Irradiation Experiment

Blaise P. Collin, Paul A. Demkowicz, David A. Petti,
Grant L. Hawkes, Joe Palmer, Binh T. Pham, Dawn M. Scates, James W. Sterbentz
Idaho National Laboratory
2525 Fremont Avenue, Idaho Falls, ID 83415, USA
Phone: +1-208-526-2217, blaise.collin@inl.gov

Abstract – *AGR-3/4 was the combined third and fourth planned irradiations for the U.S. Department of Energy (DOE) Advanced Gas Reactor (AGR) Fuel Development and Qualification Program. The primary purpose of the AGR program is to support the development and qualification of tristructural isotropic (TRISO)-coated particle fuel for use in High Temperature Gas-cooled Reactors. AGR-3/4 was designed as a fission product transport irradiation experiment whose specific objectives were to: (1) irradiate fuel containing UCO (uranium oxycarbide) designed-to-fail (DTF) fuel particles that provide a fixed source of fission products for subsequent transport through compact matrix and structural graphite materials; (2) assess the effects of sweep gas impurities on fuel performance and fission product transport; (3) provide irradiated fuel and material samples for post-irradiation examination (PIE) and post-irradiation heating; and (4) support the refinement of fuel performance and fission product transport models. The AGR-3/4 test train was irradiated in the northeast flux trap of the Advanced Test Reactor (ATR) at Idaho National Laboratory (INL) for 369.1 effective full power days from December 2011 to April 2014. The experiment was successful in achieving its specification goals in terms of burnup and fast fluence levels reached at the end of irradiation and fuel temperature levels maintained throughout irradiation: peak compact burnup reached 15.27% fissions per initial heavy-metal atom and peak compact fast fluence reached 5.32×10^{25} n/m^2 ($E > 0.18$ MeV), while the time-average volume-average temperatures of the compacts ranged from 854 to 1345°C. Fission product release-to-birth ratios reached values in the 10^{-4}-10^{-3} range early during irradiation as the DTF particles started to fail. Subsequent post-irradiation examination will provide information on fission product distributions in matrix and core graphite materials, enabling refinement of fission product transport models.*

1. Introduction

The U.S. Department of Energy (DOE) Advanced Gas Reactor (AGR) Fuel Development and Qualification Program is pursuing the development and qualification of tristructural isotropic (TRISO)-coated particle fuel for use in High Temperature Gas-cooled Reactors (HTGRs). The AGR fuel program consists of a series of irradiation experiments of TRISO fuel in the Advanced Test Reactor (ATR) at Idaho National Laboratory (INL), followed by post-irradiation examination (PIE) and safety testing campaigns. The goals of the AGR irradiation experiments are to provide irradiation performance data to support fuel process development, qualify fuel for normal operating conditions, support development and validation of fuel performance and fission product transport models and codes, and provide irradiated fuel and materials for PIE and safety testing (Petti et al., 2010).

AGR-3/4 was designed as a fission product transport irradiation experiment whose specific objectives were to: (1) irradiate fuel containing UCO (uranium oxycarbide[1]) designed-to-fail (DTF) fuel particles that provide a fixed source of fission products for subsequent transport through compact matrix and structural graphite materials; (2) assess the effects of sweep gas impurities, such as CO, H_2O, and H_2 typically found in the primary coolant circuit of HTGRs, on fuel performance and fission product transport; (3) provide irradiated fuel and material samples for PIE and safety testing; and (4) support the refinement of fuel performance and fission product transport models with on-line and PIE data. The primary objective of the test was directed towards providing data on fission product transport from particles with failed coatings using DTF particles. From the irradiation and PIE, data on fission product

[1] Uranium oxycarbide is a heterogeneous mixture of uranium oxide and uranium carbide.

diffusivities in fuel kernels and sorptivities and diffusivities in compact matrix and structural graphite materials will be derived for use in the refinement of fission product transport models. These models are needed to evaluate the fission product source term in HTGRs and support their design, safety analyses, and licensing.

2. Experimental approach

2.1. AGR-3/4 fuel and irradiation

Fuel for AGR-3/4 consisted of UCO unaltered "driver" fuel particles and UCO DTF fuel particles. The driver fuel consisted of TRISO–coated particles very similar to the baseline fuel particles used in the AGR-1 experiment (Demkowicz et al., 2016). The particles were slightly less than 1 mm in diameter with a central kernel containing low-enriched UCO fuel (nominal diameter 350 μm), a porous carbon buffer layer (nominal thickness 100 μm), an inner pyrolytic carbon layer (40 μm), a silicon carbide barrier coating (35 μm), and an outer pyrolytic carbon layer (40 μm). The DTF fuel consisted of UCO kernels identical to the driver fuel kernels coated with a single 20-μm-thick pyrolytic carbon seal coating fabricated with intentionally high anisotropy such that it would fail by irradiation-induced kernel swelling and pyrocarbon shrinkage and subsequent cracking (Miller and Knudson, 2006), providing a source of fission products to migrate from the exposed kernel through the surrounding materials. After coating, the AGR-3/4 fuel was formed into right cylindrical compacts. The compact matrix material was composed of natural and synthetic graphite powders and a thermosetting phenolic resin. Prior to compacting, the fuel particles were overcoated with thick layers of the compact matrix material. This overcoat was intended to prevent particle-to-particle contact and help achieve the desired packing fraction of fuel particles. AGR-3/4 compacts were nominally 12.5 mm in length and 12.3 mm in diameter. Each compact contained approximately 1872 driver fuel particles (average number calculated from the average uranium loading per compact and average uranium content of a particle based on its average kernel diameter and density) and exactly 20 (hand-counted) DTF particles, distributed roughly along the axial centerline of the compact as shown in Fig. 1. Details about fabrication and characterization of the driver and DTF fuel particles and the fuel compacts can be found in Hunn et al. (2014). The main characteristics of the AGR-3/4 TRISO fuel particles and compacts are summarized in Table 1 and detailed in the AGR-3/4 Irradiation As-Run Report (Collin, 2016).

The AGR-3/4 test train was irradiated in the 133.4-mm-diameter northeast flux trap of the ATR (see Fig. 2). Compared to the Large B positions used for AGR-1 and AGR-2, the larger diameter provides greater flexibility for test train design, significantly enhancing the capability for the combined irradiations. Specifically, the AGR-3/4 irradiation in the northeast flux trap position: (1) maximized space for different fission product retention materials; (2) minimized irradiation time due to a higher irradiation flux; (3) minimized the radial flux gradient across the test train; and (4) allowed power level control, as corner lobes of the ATR are controlled independently (ATR, 2009). In addition, the rate of burnup and fast fluence accumulation in this position was approximately three times that expected in HTGRs, resulting in only modest acceleration of the irradiation. This acceleration factor was high enough to accomplish the irradiation in the ATR within a reasonable time, yet low enough to avoid possible premature fuel particle failures (i.e., loss of integrity of the three outer coating layers resulting in an exposed kernel and a free path to fission product release) while still being representative of an irradiation in a full-scale reactor.

The AGR-3/4 test train was a multi-capsule, instrumented lead experiment containing twelve separate stacked capsules, each independently controlled for temperature and independently monitored for fission product gas release. Each AGR-3/4 capsule contained four fuel compacts in a single vertical stack, surrounded by three concentric annular rings of test material (see Fig. 3 and 4): (1) an annulus of fuel-compact matrix material (matrix ring of as-fabricated thickness 5.0 to 6.0 mm)[2]; (2) an annulus of fuel-element graphite (4.5 to 7.6 mm graphite ring); and (3) an annulus of graphite operating at lower temperature to act as a sink for fission products (9.6 to 12.1 mm graphite sink). The thicknesses of the rings were designed to be adequate to study the diffusion of fission products in matrix and graphite materials. The materials used to fabricate the AGR-3/4 graphite rings and sinks were two candidate nuclear-grade graphites considered for high-dose regions in conceptual high temperature reactors: IG-110 (Capsules 8 and 9) and PCEA (remaining capsules). IG-110 is an isostatically molded graphite with a very fine grain structure, whereas PCEA is an extruded graphite. Table 2 shows a summary of the graphite materials for the different rings in each AGR-3/4 capsule.

[2] While the majority of the capsules used an inner ring of matrix material as described here, the matrix ring was replaced with a graphite ring in three of the capsules (Capsules 3, 8, and 10) in order to obtain additional data on fission product transport in graphite at higher temperature.

The entire assembly of compacts and rings was inside a stainless steel shell that acted as the pressure boundary. Outside each capsule shell, a thin metal sheet (called a "shroud") of hafnium was used as a filter used to shape the temporal and spatial fuel power distribution and reduce the ratio of maximum to minimum heat generation rates in the fuel, which facilitated temperature control of the test train during irradiation and ensured the temperature requirements of the experiment were met. The graphite sink was penetrated by through tubes, which provided passage for thermocouples used for temperature measurement within the capsule, and gas lines to be routed to each of the twelve capsules. A leadout tube housed the gas lines and thermocouple leads between the top of the upper capsule and the reactor vessel penetration wall. Outside the reactor vessel, these gas lines and thermocouple leads were connected to their respective facility counterparts in the temperature monitoring, control, and data acquisition system.

The AGR-3/4 experiment was designed as a time-at-temperature experiment in which each capsule is thermally controlled in a range of temperatures suitable for the measurement of the diffusion of fission products. To meet the dual objectives of studying fission product release from the fuel and retention in the matrix and/or the graphite, temperature control was performed on fuel for six capsules and on graphite for the other six capsules. Specifically, Capsules 1, 3, 6, 7, 11, and 12 were controlled on peak fuel temperature, while Capsules 2, 4, 5, 8, 9, and 10 were controlled by maintaining their matrix ring or graphite ring mid-points within set ranges of temperatures. Table 3 shows the temperature matrix that was planned prior to the start of irradiation.

Temperature control was achieved by routing a mixture of helium and neon gases through each of the twelve capsules by independent gas lines. The gas mixture was also used to sweep the fission gases released in each capsule during irradiation and carry them to the Fission Product Monitoring System for analysis (see Section 2.4). Temperature control was based upon temperature feedback from the thermocouples in each capsule and performed by varying the sweep gas composition (between 100% helium for high conductivity and 100% neon for low conductivity). There were four annular gas gaps between components in each capsule, numbered 1 through 4 (see Fig. 3). Two of these gaps provided the primary means of temperature control in the capsules: Gap 3 between the graphite ring and the graphite sink and Gap 4 between the graphite sink and the stainless steel capsule shell. The capsule temperature was primarily dictated by the heat transfer across these two control gaps. The purpose of the dual control gaps was to run the sink at a much cooler temperature, resulting in effective fission product retention, and to decrease the operating temperature of the instrumentation placed in the sink, resulting in a prolonged life of the thermocouples in this ring. The gas gaps between the other layers were set to a fixed minimum width to minimize the temperature difference between the layers, except in Capsule 11, where Gap 2 was made slightly wider so that a higher temperature was achieved in the matrix ring. Reactor coolant water flowed on the outside of the stainless steel capsule shell. The blending of sweep gases was accomplished by a computerized mass flow controller before the gas entered the test train. In addition to the helium and neon sweep gas mixture necessary to provide thermal control of the experiment, Capsule 11 was injected with impurities (i.e., 50 ppmv CO, 10 ppmv H_2O, and 50 ppmv H_2) typically found in the primary coolant circuit helium of HTGRs. These impurities were injected in Capsule 11 during the last three cycles of the irradiation (ATR cycles 8 to 10) to assess their effects on fuel performance and fission product transport. Fig. 5 shows a schematic diagram of the gas flow path.

Temperature was measured by thermocouples located in the matrix ring and graphite sink. Calculated temperatures from as-run thermal analyses (see Section 2.3.1) were compared to the thermocouple readings to ensure reliable temperature predictions for each following cycle. Temperature control ensured that temperatures in the capsules were maintained at their set point values, which guaranteed fuel or matrix/graphite temperatures were kept at the requisite levels. Each capsule housed two thermocouples in the graphite sink, one of which was designated as the control thermocouple. Three capsules (Capsules 5, 10, and 12) had an additional thermocouple in the matrix ring (see Fig. 6). All thermocouples terminated at the midplane of the fuel stack. When a control thermocouple failed during irradiation, the other sink thermocouple within the same capsule was used as the control thermocouple and the control temperature set point was reset based on thermal analysis calculations. When all thermocouples failed within a capsule, results of thermal analyses were used to manually set the gas blends of the affected capsule.

The AGR-3/4 irradiation experiment lasted from December 2011 to April 2014, which spanned a total of ten ATR cycles. The third of the ten cycles was a low-power cycle during which no burnup was accumulated. The fifth cycle included an unplanned outage (the reactor was not operated) during which the AGR-3/4 test train was

temporarily removed from the reactor. It remained out of the reactor for the sixth cycle (a Power Axial Locator Mechanism, or PALM, cycle) in order to prevent over-heating of the fuel compacts, and was reinserted for cycles 7-10. During the seven normal power cycles for which the test train was in the reactor, the experiment was irradiated for a total of 369.1 effective full power days (EFPD). The power in the northeast lobe was progressively increased from 14 to 19 MW during the course of the AGR-3/4 irradiation to maintain temperature in capsules as the U-235 depleted.

2.2. Physics analysis

Detailed as-run physics depletion calculations were performed after each irradiation cycle using a sophisticated three-dimensional, fully-explicit Monte Carlo N-Particle (MCNP) model of the entire ATR core and AGR-3/4 experiment (Sterbentz, 2015). Neutron spatial flux distributions, nuclear reaction rates, fission and radiation energy deposition rates, burnups, fast neutron fluences, and fission product and actinide concentrations were calculated in every compact at each time step (~24-hour), similar to the physics depletion calculation performed for AGR-1 (Sterbentz et al., 2015). Some of these calculated data were then used for thermal and fission product gas release analyses (see Sections 2.3 and 2.4) and fuel performance and fission product transport modeling activities.

The Monte Carlo depletion methodology was based on the coupling of the MCNP transport code (LANL, 2003) and the depletion code ORIGEN2.2 (Croff, 1983) by the JMOCUP utility program (Babcock et al., 1994; Sterbentz et al., 2010). Temperature-dependent neutron cross sections were also generated by the nuclear data processing system NJOY (MacFarlane and Boicourt, 1975) for use in the AGR-3/4 model description. Calculations were performed using a so-called particle model, which placed the uranium in discreet spheres (e.g., the fuel kernels). This model allowed for self-shielding of U-238 in the kernels and was expected to produce more accurate isotopic concentrations for actinides and fission products compared to earlier models that assumed uniform distribution of uranium throughout the compact volume. Each AGR-3/4 compact was subdivided into two equal-volume axial depletion cells, with each cell containing seven layers of particles and each layer containing 135 particles, or 945 particles per cell and 1890 particles per compact. The particle model calculated the data averaged over each of the two compact depletion cells. The graphite annuli (i.e., matrix, ring, and sink) were subdivided into four azimuthal quadrants. The AGR-3/4 JMOCUP calculation depleted three zones: (1) ATR driver core, (2) AGR-3/4 TRISO compacts, and (3) AGR-3/4 hafnium capsule shroud. The meshing of these three zones in the MCNP model required a total of 984 depletion cells. MCNP calculated the neutron flux and reaction rates for each isotope in each depletion cell to provide one-group cross sections that were then used in ORIGEN2.2 depletion calculations. JMOCUP tracked or updated the fission, radiative capture, (n,2n), (n,3n), (n,p), and (n,α) nuclear reaction cross sections for both actinides and fission products at each calculation time step in each depletion cell. In the 840 ATR driver fuel depletion cells, nine actinides and 24 fission product isotopes were tracked. In the 96 fuel compact depletion cells, 21 actinides and 71 fission products were tracked. In the hafnium shroud cells, the six naturally occurring hafnium isotopes were tracked.

The ATR power cycles were subdivided into daily (~24-hour) time steps over the 369 EFPDs of the AGR-3/4 irradiation. At each time step, daily average values of the ATR measured reactor data, which included total core power, lobe powers, outer shim control cylinder positions, and removal of the neck shim rods, were used to deplete the three zones and calculate all of the above-mentioned physics data. The depletion calculation using JMOCUP closely mimicked the criticality (k-effective ≈ 1.0) of the actual ATR core. The main results of these AGR-3/4 physics calculations (i.e., compact burnup and fast fluence) are discussed in Section 3.

As part of the AGR-3/4 PIE, the inventory of selected gamma-emitting isotopes in the compacts and the compact burnup (including axial burnup profiles) are being determined by gamma spectrometry. Isotopic inventory of additional fission products and actinides will also be measured by destructive examination of particles using mass spectrometry, including U and Pu isotopic inventories. In addition, flux monitor wires embedded in the capsules will be analyzed to determine total neutron fluence at these locations. These data will be compared to the physics calculations in order to validate the AGR-3/4 physics model. The results of these comparisons will be presented in a separate publication.

2.3. Thermal analysis

Evaluating the thermal conditions of the fuel during irradiation is an essential component of assessing its performance. The AGR-3/4 experiment was designed as a time-at-temperature experiment in which each capsule is thermally controlled in a range of temperatures suitable for the measurement of the diffusion of fission products. To meet the dual objectives of studying fission product release from the fuel and retention in the matrix and/or the graphite, temperature control was performed on fuel for six capsules and on graphite for the other six capsules. The goal of the thermal predictions was to adjust the thermocouple set points as the fuel burned during irradiation to determine the proper sweep gas mixture required to maintain target fuel or graphite temperature. Heat rates calculated by physics analysis were used to predict the temperature at which the AGR-3/4 fuel compacts were irradiated, since thermocouples could not be used directly on the fuel compacts.

2.3.1. Thermal calculation methodology

The Abaqus finite element stress and heat transfer code (Abaqus, 2014) was used to perform the daily as-run thermal analysis of the AGR-3/4 capsules (Hawkes, 2015; Hawkes et al., 2015). These calculations were performed using compact and graphite heat generation rates and fast neutron fluence provided by the physics analysis (see Section 2.2) and with additional operational input for daily helium-neon gas mixture composition and flow rate. Each AGR-3/4 capsule was described by a finite element mesh formed from approximately 400,000 eight-node hexahedral brick elements (see Fig. 7). Each compact was discretized with ~3,500 of such brick elements.

The fuel compact thermal conductivity was taken from historical correlations that take into account temperature of heat treatment, irradiation temperature, fast neutron fluence, and TRISO particle packing fraction (Gontard and Nabielek, 1990). The thermal conductivity was scaled according to the ratio of the AGR-3/4 compact matrix density (1.6 g/cm^3, respectively) to the compact matrix density used to develop the correlations (1.75 g/cm^3) to adjust for density differences. It was then combined with particle thermal conductivity obtained from Folsom et al. (2015), following an approach described by Gonzo (2002) to obtain an effective thermal conductivity for the compact at a given TRISO particle volume packing fraction (where packing fraction is defined as the total volume of particles divided by the total volume of the compact). The thermal conductivity of the matrix ring was taken from the fuel compact thermal conductivity correlation with a packing fraction of zero because no pure matrix material conductivity was available. The thermal conductivities of the unirradiated IG-110 and PCEA graphites were derived from measurements of their thermal diffusivities at INL (Collin, 2016). The effect of irradiation on the thermal conductivity of the graphite was accounted for using a correlation by Snead and Burchell (1995).

Heat produced in the fuel compacts and graphite rings was transferred through the gas gaps surrounding the compacts and rings via a gap conductance model using the gap width and the conductivity of the sweep gas. Heat transfer across every gap was considered by both radiation (15-20% of the heat transfer depending on the temperature of the compacts) and conduction (80-85%). Because the thermal capacitance of the sweep gas is very low, advection was not considered in the sweep gas and it was modeled as stationary. The convective heat transfer from the sweep gas would be <0.01% of the heat transfer across the gap because of the low density, low flow rate, and low thermal capacitance. The thermal conductivity of the sweep gas was determined using a set of correlations from Brown University for mixtures of noble gases (Kestin et al., 1984). All gas gaps were modeled as changing linearly with time in response to the graphite dimensional change with fast neutron fluence. This was accomplished by having the gas gap conductivity of each capsule change with fast neutron fluence (Hawkes, 2015; Hawkes et al., 2015).

The thermal model provided daily temperature distributions for all the components of the AGR-3/4 capsules. Fig. 8 shows such a typical distribution for Capsule 12. The main results of these AGR-3/4 thermal calculations (e.g., compact and annular ring temperatures) are discussed in Section 3.

2.3.2. Sensitivity evaluation of the thermal model

A temperature sensitivity evaluation was performed for one of the AGR-3/4 capsules (Capsule 5) to assess the sensitivity of the daily thermal predictions to the various input parameters of the thermal model (Hawkes et al., 2015). Input parameters were varied by ±10% to show the temperature sensitivity to each parameter. The major parameters affecting the thermal results were found to be the fuel compact heat rate, the gas mixture (neon fraction), the gas gaps varying with fluence, and the fuel compact conductivity.

Table 4 shows the best-estimate uncertainties for these parameters. These uncertainty values are based on machining tolerances, physics code calculations, mass flow controllers, and engineering experience. Fig. 9 shows the results of this sensitivity study for the peak fuel temperature of AGR-3/4 Capsule 5, as calculated in a base case representing one particular day of the entire irradiation. The peak fuel temperature of Capsule 5 was ~1124°C in that base case. Fig. 9 shows that a ±10% variation of the fuel compact heat rate results in a total variation of the peak temperature of 89°C. Similarly, the total peak fuel temperature variations resulting from ±10% variation of the neon fraction, width of the outer control gas gap, and fuel compact conductivity are 48, 21, and 20°C respectively. The sensitivity evaluation of the thermal model was used to support quantification of the uncertainty in the AGR-3/4 calculated temperatures (Pham et al., 2016a).

2.4. Fission product gas release analysis

The AGR-3/4 experiment was designed to provide a geometrically defined line source of fission products from DTF particles. This allowed a simple configuration to model fission product release since their location along the compact centerline helped to minimize the range of temperature, burnup, and fast fluence that the DTF particles experienced in a given compact. Monitoring of their failures, by detection of released gaseous fission products throughout the AGR-3/4 irradiation, was performed by the Fission Product Monitoring System (FPMS) developed at INL (Scates et al., 2010).

The FPMS incorporated fourteen individual monitoring systems, one for each of the individual capsule effluent lines, and two units that could monitor any individual effluent line or any combination of up to six lines (see Fig. 5). The two additional monitors were primarily provided as backup units capable of providing effluent line monitoring should any of the primary monitoring systems fail. Each monitor consisted of a high purity germanium gamma-ray spectrometer used for isotopic quantification of the noble gas release and a sodium iodide scintillation detector used to detect the failure of individual TRISO or DTF particles by measuring the total gross gamma counts from capsule specific effluent. The scintillation detector counting rate was monitored using a computer-controlled multi-channel scaler. The system was designed to detect up to 250 individual particle failures from each capsule. The FPMS continuously measured the isotopic fission gas content of the sweep gas from each AGR-3/4 capsule, thereby providing an indication of fuel irradiation performance. The sweep gas from each test capsule was routed via sampling lines to the monitoring station associated with that capsule. Spectrometer systems then measured the concentrations of various krypton and xenon isotopes in the sweep gas from each capsule to assess the release of these noble gases and detect potential TRISO particle failures. Krypton and xenon release is a good indicator of particle failure because, unlike other main fission products, their diffusivities in pyrocarbon are very low. Therefore, a particle with an intact pyrocarbon layer releases krypton and xenon at a very slow rate, while a burst in krypton and xenon release indicates the loss of integrity of all the coating layers of a driver fuel particle or of the single pyrocarbon seal coating layer of a DTF particle.

Physics calculations provided as-run fission product birthrates for select krypton and xenon isotopes. The selected nuclides (i.e., Kr-85m, Kr-87, Kr-88, Kr-89, Kr-90, Xe-131m, Xe-133, Xe-135, Xe-135m, Xe-137, Xe-138, and Xe-139) were chosen because they are chemically inert fission product gases with relatively short half-lives, allowing each isotope to reach equilibrium concentration in the fuel during each reactor cycle. Data obtained from the FPMS were used to calculate the R/B ratios for the radionuclides of interest (Scates, 2015). In the case of the AGR-3/4 experiment, the detection of fission gas release also served to monitor the failure count of the DTF particles. The main results of this AGR-3/4 fission product gas release analysis (R/B ratios and DTF fuel failure count) are discussed in Section 3.

2.5. AGR-3/4 operational issues

To maintain temperature in the capsules as the fissile material depleted, the power in the ATR northeast lobe was increased during the course of the AGR-3/4 irradiation. A progressive power increase ensured that the temperature control could be maintained by the helium-neon sweep gas mixture as the fissile fuel content was consumed and the heat generation rate dropped. Consequently, the northeast lobe power was increased from about 14 MW (cycles 1 and 2) to about 16 MW (cycles 4 and 7), and then to about 18 MW (cycles 8 and 9), and finally to about 19 MW (cycle 10). Cycle 3 was a low-power cycle, Cycle 5 was an unplanned outage, and Cycle 6 was a PALM cycle during which the northeast lobe power was set to 20 MW. The AGR-3/4 test train was removed from the reactor during these Cycle 5 and Cycle 6.

As mentioned in Section 2.3, half of the capsules were controlled on peak fuel temperature, while the other half were controlled by maintaining their matrix ring or graphite ring mid-points at a constant temperature. The target values for all capsules are given in Table 3. The objective of the AGR-3/4 experiment was to maintain the control temperatures as constant as possible throughout irradiation. As full power was achieved at the beginning of the first AGR-3/4 cycle, the temperatures reached in the capsules differed somewhat from the expected values of Table 3, which after the fact was traced to incomplete physics models used in the design of the capsule that resulted in incorrect thermal predictions. Subsequently, these observed values were used as target temperatures for the first three cycles, superseding the target values from Table 3. Nevertheless, the control temperatures remained relatively constant throughout these first three cycles. New thermal calculations were performed that included a complete physics model and incorporated modeling of varying gap width with irradiation (see Section 2.3.1). These new thermal predictions showed good agreement with the thermocouple measurements from the first three cycles. They were deemed appropriate to determine the target control temperatures for the last four cycles of the AGR-3/4 experiment. This was done by setting the target values to the average values of the calculated control temperatures of the first three cycles. Temperature bands of ±75°C and ±50°C were defined for peak fuel temperature and graphite temperature, respectively, as acceptable boundaries for variation of the control temperatures around their target values. Control temperatures in the capsules were successfully kept in the temperature bands around their respective targets in most cycles, although temperatures in the middle capsules (Capsules 4 to 9) started to increase upwards and outside their control bands during the last two AGR-3/4 cycles (see Fig. 10 and Fig. 11). The increase was the consequence of an operational increase in the capsule temperatures in response to a drop in the gross gamma signal. This was indicative of a decrease in fuel temperatures from fuel depletion, which was not predicted by thermal calculations based on measurements from the thermocouples situated farther away in the capsule rings. When gross gamma detectors and calculated temperatures obtained from thermocouple readings started providing conflicting indications, gross gamma signal was used as an indicator of fuel temperatures, as it was deemed more reliable than the thermal predictions at this point of the experiment. The helium-neon gas mix was adjusted accordingly and it led to higher calculated control temperatures that ended up overshooting their operating bands. Nevertheless, the rise of calculated temperatures towards the end of irradiation did not jeopardize the objectives of the experiment.

The AGR-3/4 thermocouples performed relatively well – of the 27 installed thermocouples, only five failed during irradiation. All capsules, except Capsule 3, retained a control thermocouple for the duration of the irradiation. Small diameter thermocouples (1.5 mm), such as those used in AGR-3/4, deteriorate and sometimes fail because of the relatively high neutron flux and elevated temperatures that occur during test reactor cycles. The relatively high thermocouple longevity in this experiment, as compared to the earlier AGR-1 and AGR-2 experiments, is primarily attributed to their placement in lower-temperature locations in the AGR-3/4 capsule. All thermocouple failures were attributed to open circuit failure, which is typically caused by breakage of a thermo-element wire or the junction itself. After both thermocouples in Capsule 3 failed near the end of the eighth cycle, the neon fraction in the gas mixture was set to 0.52 for the rest of the cycle and increased to 0.68 for the last two cycles, as the fuel heat rate started to decrease. Thermal analysis showed that the projected peak fuel temperature could be maintained within the desired control band of 1250±75°C with that neon fraction of 0.68.

3. AGR-3/4 experiment results

Tables 5 and 6 show the minimum, capsule-average (i.e., average of four compacts), and peak values for calculated compact burnup and fast fluence at the end of irradiation, as well as the goals specified during the design of the experiment. These tables show that burnup on a compact basis ranged from 4.85 to 15.27% FIMA and the compact fast fluence ranged from 1.19×10^{25} to 5.32×10^{25} n/m^2 (E > 0.18 MeV). On a capsule basis, capsule-average burnup ranged from 5.35% FIMA in Capsule 12 to 15.24% FIMA in Capsule 6, while capsule-average fast fluence ranged from 1.50×10^{25} n/m^2 (E > 0.18 MeV) in Capsule 12 to 5.31×10^{25} n/m^2 (E > 0.18 MeV) in Capsule 6.

Fig. 12 and Fig. 13 show the calculated daily fuel temperatures for the twelve capsules of the AGR-3/4 test train. They remained constant for most of the irradiation, with the exception of the increase in the middle capsules during the last 105 days of irradiation (i.e., the last two cycles, see Section 2.5). Table 7 shows the corresponding time-average minimum, capsule-average (average of the time-average volume-average temperatures of the four compacts), and time-average peak temperatures at the end of irradiation, as well as the temperature goals for the

twelve capsules. It shows that the time-average volume-average temperatures on a capsule basis ranged from 854°C in Capsule 12 to 1345°C in Capsule 7.

Fig. 14 and Fig. 15 show the daily differences between the measured and calculated thermocouple (TC) temperatures. There is a good agreement with most differences within approximately ±60°C. Exceptions include both thermocouples in Capsule 11 (differences as large as -90°C), TC-2 in Capsule 7 and TC-1 in Capsule 4 (differences as large as +90°C), and TC-3 in Capsule 5 (difference of up to 120°C).

Fission product R/B values ranged from 10^{-4} to 10^{-3} early during irradiation as DTF particles started to fail during the first AGR-3/4 cycle (see Fig. 16 and Fig. 17). The hotter Capsule 7 reached the highest R/B value of around 3×10^{-3}. Table 8 shows the count per capsule and includes minimum and maximum counts in addition to the best-estimate count. Even though the gross gamma detector is sensitive to each fuel particle failure (up to 250 failures), visually counting the exact number of failed particles during the whole AGR-3/4 irradiation was a challenging task because of the ongoing release from already failed DTF particles. These challenges led to uncertainty in the particle failure counts in some capsules and, therefore, three estimates (i.e., minimum, best-estimate, and maximum) were provided for the failure counts. Fig. 18 plots the weekly cumulative best-estimate failure counts as a function of EFPDs for each of the twelve AGR-3/4 capsules. For most capsules, the majority of the fuel failures occurred during the first irradiation cycle (e.g., within the first 55 EFPDs). For a few of the capsules (e.g., Capsules 2 and 3), the timing of fuel failures was more distributed throughout irradiation. Based on best-estimate values, the final particle failure count ranges from 39 (i.e., Capsule 12) to 96 (i.e., Capsule 3) of the initial 80 DTF particles in each capsule (i.e., 20 DTF particles in each of four compacts per capsule). In particular, Capsules 2, 3, and 9 each have a final best-estimate failure count higher than 80 DTF particles. Since each compact was loaded with exactly 20 DTF particles (see Section 2.1), any uncertainty on the initial number of DTF particles per capsule can be ruled out. Failures of DTF particles cannot be distinguished from potential failures from driver fuel particles based on measured fission gas release during the experiment. However, based on the AGR-1 irradiation fuel performance that resulted in zero particle failures out of $\sim3\times10^5$ particles (Grover et al., 2010) and the similarities between the irradiation conditions of the similar AGR-1 and AGR-3/4 fuels, it is reasonable to assume that significant in-pile failure was unlikely among the $\sim9\times10^4$ qualified AGR-3/4 driver fuel particles. Since the goal of the AGR-3/4 experiment was to provide a source of fission products for fission product transport analyses, the integrity of the driver fuel was not of primary importance. Thus, the total number of fuel particle failures in each AGR-3/4 capsule was capped at a maximum of 80 failures for use in fission product data analysis. For the most part, the uncertainty in the number of failed DTF particles only generates a limited uncertainty in the fission product source term because the PyC seal coating layer of the DTF particles is mostly little retentive of the radiologically significant fission products of interest – silver, cesium, strontium, and europium. In this scenario, intact and failed DTF particles release similar amounts of these fission products throughout irradiation. This statement applies to silver, strontium, and europium over the entire range of the AGR-3/4 irradiation temperatures and to cesium at the upper end of this temperature range. At lower temperatures, the PyC seal acts as a potent barrier to cesium diffusion so the uncertainty in the number of failed DTF particles can generate an uncertainty in the amount of cesium released. However, in all cases, the impact on fission product transport analysis is minor because the source term uncertainty is dominated by the uncertainty on the contribution from fission products released from intact particles. This contribution cannot be reliably distinguished experimentally from the release from DTF particles. Furthermore, it is not accurately predicted by fission product transport models because of large uncertainties on diffusion coefficients in TRISO particles and matrix material.

The measured R/B ratios of the AGR-3/4 irradiation were used in a fission gas release-to-birth ratio data analysis of the AGR-2 and AGR-3/4 experiments whose goal was to determine an R/B correlation giving the R/B per failed particle as a function of reciprocal temperature (Pham et al., 2016b). The resulting R/B correlation compares favorably to historical data and lies below the intentionally conservative R/B models currently used in most TRISO fuel performance codes. This R/B correlation can be used by reactor designers to estimate fission gas release from postulated failed fuel in HTGR cores, which is the key safety factor for fuel performance assessment.

As mentioned in Section 2.1, impurities (i.e., carbon monoxide, water, and hydrogen) were added to the sweep gas and injected in Capsule 11 during the last three cycles of AGR-3/4 (ATR cycles 8 to 10) to assess their effects on fuel performance and fission product transport. Very small quantities of iodine isotope I-131 were identified in gamma spectra from the Capsule 11 outlet flow several days after the end of ATR cycle 8. Throughout irradiation, these spectral lines were mostly obscured by the gamma lines from the mobile krypton and xenon isotopes. During

ATR irradiation cycle 8, the I-131 activity in the FPM 11 sample chamber peaked at about 2.3×10^{5} Bq. While this was a notable increase in measured activity at the detector, this value represents a fraction of only 6×10^{-7} of the expected I-131 inventory produced in the capsule reaching the FPM. The increase in I-131 in FPM 11 with the addition of the impurities during ATR cycle 8 strongly suggests that the impurities were helping to mobilize some of the I-131 capsule inventory. As a check, impurity injection was halted early during ATR cycle 10. When the reactor unexpectedly scrammed at mid-cycle, the level of activity was consistent with an iodine-free inventory. Impurities were then re-injected at reactor start-up following the scram. Two weeks later, at the end of the cycle, the activity had increased, showing that iodine had been again mobilized, although at a lower level than at the end of the two previous cycles (Scates et al., 2014).

4. Conclusions

The AGR-3/4 fuel irradiation was successful in achieving the burnup, fast fluence, and temperature goals for its fuel compacts (see Tables 5 to 7):

- Compact burnup ranged from 4.85 to 15.27% FIMA.
- Compact fast fluence ranged from 1.19 to 5.32×10^{25} n/m^2 (E > 0.18 MeV).
- Time-average volume-average fuel temperatures on a capsule basis at the end of irradiation ranged from 854°C in Capsule 12 to 1345°C in Capsule 7.

The AGR-3/4 experiment was successful in keeping the control temperatures of the twelve capsules relatively constant in a range of temperatures suitable for measurement of fission product diffusion in compact matrix and structural graphite materials, thanks to an efficient capsule design and to the power flexibility of the northeast lobe. Most DTF particles failed as expected, although some capsules (Capsules 6, 7, 10, and 12) had an estimated maximum failure count smaller than the initial loading of 80 DTF particles per capsule. Nevertheless, the DTF failures provided a source of fission products for post-irradiation fission product transport analysis, as intended. In addition, the thermocouples performed relatively well: of the 27 installed thermocouples, only five failed late during operation. Fission product R/B values ranged from 10^{-4} to 10^{-3} early during irradiation as DTF particles started to fail during the first AGR-3/4 cycle. The hotter Capsule 7 reached the highest R/B value of around 3×10^{-3}. Impurities added to the sweep gas did not seem to have an appreciable impact on fuel performance or fission product transport, but very small quantities of iodine isotope I-131 were identified in the sweep gas following the injection of the impurities and its transport to the detection system is believed to have been facilitated by the injected moisture.

The results of this test provide irradiation performance (R/B per failed particle) and fission product transport data. PIE for this experiment focuses on: (1) determining the extent of fission product migration in the matrix and graphite rings during irradiation; (2) determining the extent of fission product migration in the matrix and graphite rings at elevated temperatures during heating in pure helium; (3) evaluating retention of fission products in fuel kernels and compact matrix during irradiation; and (4) determining the extent of condensable and gaseous fission product release from fuel kernels and compact matrix at elevated temperatures during heating in pure helium. PIE work has started and metrology data on graphite dimensional changes were used to refine the AGR-3/4 thermal calculations (Hawkes et al., 2017) which are needed for fission product transport analysis (Humrickhouse et al., 2016). Once PIE is completed, this test will yield useful data on fission product diffusion, which are crucial for modeling of fission product transport and release from the reactor core during operation and during reactor accident scenarios. These models are needed to evaluate the fission product source term in HTGRs and support their design, safety analyses, and licensing.

Acknowledgments

This submitted manuscript was authored by a contractor of the U.S. Government under DOE Contract No. DE-AC07-05ID14517. Accordingly, the U.S. Government retains and the publisher, by accepting the article for publication, acknowledges that the U.S. Government retains a nonexclusive, paid-up, irrevocable, world-wide license to publish or reproduce the published form of this manuscript, or allow others to do so, for U.S. Government purposes.

References

Abaqus, 2014. Abaqus Version 6.14-2 documentation. Dassault Systèmes.

ATR, 2009. FY 2009 Advanced Test Reactor National Scientific User Facility Users' Guide. INL/EXT-08-14709, Idaho National Laboratory (INL).

Babcock, R.S., Wessol, D.E., Wemple, C.A., Mason, S.C., 1994. The MOCUP interface: A Coupled Monte Carlo/depletion system. Proceedings of the Topical Meeting on Advances in Reactor Physics, Knoxville, Tennessee, USA, April 11-15.

Collin, B.P., 2016. AGR-3/4 Irradiation As-Run Final Report. INL/EXT-15-35550, Rev. 1, Idaho National Laboratory (INL).

Demkowicz, P.A., Hunn, J.D., Petti, D.A., Morris, R.N., 2016. Key results from irradiation and post-irradiation examination of AGR-1 UCO TRISO fuel. Proceedings of the 8th International Topical Meeting on High Temperature Reactor Technology (HTR 2016), Las Vegas, Nevada, USA, November 6-10.

Croff, A.G., 1983. ORIGEN2: A Versatile Computer Code for Calculating the Nuclide Compositions and Characteristics of Nuclear Materials. Nuclear Technology, 62, 335-352.

Folsom, C., Xing, C., Jensen, C., Ban, H., Marshall, D.W., 2015. Experimental measurement and numerical modeling of the effective thermal conductivity of TRISO fuel compacts. Journal of Nuclear Materials, 458, 198–205.

Gontard, R., Nabielek, H., 1990. Performance Evaluation of Modern HTR TRISO Fuels. Report HTA-IB-05/90, Forschungszentrum Jülich GmbH (FZJ).

Gonzo, E.E., 2002. Estimating correlations for the effective thermal conductivity of granular materials. Chemical Engineering Journal, 90, 299–302.

Grover, S.B., Petti, D.A., Maki, J.T., 2010. Completion of the First NGNP Advanced Gas Reactor Fuel Irradiation Experiment, AGR-1, in the Advanced Test Reactor. Proceedings of the 5th International Topical Meeting on High Temperature Reactor Technology (HTR 2010), Prague, Czech Republic, October 18-20.

Hawkes, G.L., 2015. AGR-3/4 Daily As-Run Thermal Analyses. ECAR 2807, Rev. 0, Idaho National Laboratory (INL).

Hawkes, G., Sterbentz, J., Pham, B., 2015. Sensitivity evaluation of the AGR-3/4 experiment thermal model irradiated in the Advanced Test Reactor. Proceedings of the 2015 International Mechanical Engineering Congress and Exposition (IMECE 2015), Paper No. 53544, International Mechanical Engineering Congress & Exposition Conference, Houston, Texas, USA, November 13–19.

Hawkes, G.L., Sterbentz, J.W., Maki, J.T., Pham, B.T., 2017. Thermal Predictions of the AGR-3/4 Experiment With Post Irradiation Examination Measured Time-Varying Gas Gaps. Journal of Nuclear Engineering and Radiation Science, 3(4), 041007.

Humrickhouse, P.W., Collin, B.P., Hawkes, G.L., Harp, J.M., Demkowicz, P.A., Petti, D.A., 2016. Modeling and analysis of fission product transport in the AGR-3/4 experiment. Proceedings of the 8th International Topical Meeting on High Temperature Reactor Technology (HTR 2016), Las Vegas, Nevada, USA, November 6-10.

Hunn, J.D., Trammel, M.P., Montgomery, F.C., 2011. Data Compilation for AGR-3/4 Matrix Ring Blank Lot ARB-B1. ORNL/TM-2011/272, Oak Ridge National Laboratory (ORNL).

Hunn, J.D., Lowden, R.A., Miller, J.H., Jolly, B.C., Trammell, M.P., Kercher, A.K., Montgomery, F.C., Silva, C.M., 2014. Fabrication and characterization of driver-fuel particles, designed-to-fail fuel particles, and fuel compacts for the US AGR-3/4 irradiation test. Nuclear Engineering and Design, 271, 123-130.

Kestin, J., Knierim, K., Mason, E.A., Najafi, B., Ro, S.T., Waldman, M., 1984. Equilibrium and Transport Properties of the Noble Gases and Their Mixtures at Low Density. Journal of Physical and Chemical Reference Data, 13, 229–303.

LANL, X-5 Monte Carlo Team, 2003. MCNP – A General Monte Carlo N-Particle Transport Code – Version 5, LA-UR-03-1987, Los Alamos National Laboratory (LANL).

MacFarlane, R.E., Boicourt, R.M., 1975. NJOY: A Neutron and Photon Processing System. Transactions of the American Nuclear Society, 22, 720.

Miller, G.K., D.L. Knudson, 2006. An Evaluation of Design-to-Fail Particles for the AGR-3 Irradiation. EDF-7033, Idaho National Laboratory (INL).

Petti D., Maki, J., Hunn, J., Pappano, P., Barnes, C., Saurwein, J., Nagley, S., Kendall, J., Hobbins, R., 2010. The DOE Advanced Gas Reactor Fuel Development and Qualification Program. JOM 62, 62–66.

Pham, B.T., Einerson, J.J., Hawkes, G.L., 2016a. Uncertainty Quantification of the Calculated Temperatures for AGR-3/4 Experiment. INL/EXT-15-36431, Rev. 1, Idaho National Laboratory (INL).

Pham, B.T., Einerson, J.J., Scates, D.M., Maki, J.T., Petti, D.A., 2016b. AGR-2 and AGR-3/4 Release-to-Birth Ratio Data Analysis. INL/EXT-14-32970, Rev. 1, Idaho National Laboratory (INL).

Scates, D.M., Hartwell, J.K., Walter, J.B., Drigert, M.W., Harp, J.M., 2010. Fission product monitoring of TRISO coated fuel for the advanced gas reactor-1 experiment. Nuclear Engineering and Design, 240, 2493-2499.

Scates, D.M., Walter, J.B., Reber, E.L., Sterbentz, J.W., Petti, D.A., 2014. Determination of the Quantity of I-135 Released from the AGR Experiment Series. Proceedings of the 7th International Topical Meeting on High Temperature Reactor Technology (HTR 2014), Weihai, China, October 27-31.

Scates, D.M., 2015. Release-to-birth Ratios for AGR-3/4 Operating Cycles 151A through 155B. ECAR 2457, Rev. 1, Idaho National Laboratory (INL).

Snead, L.L., Burchell, T.D., 1995. Reduction in Thermal Conductivity Due to Neutron Irradiation. Extended abstracts of the 22nd Biennial Conference on Carbon, San Diego, California, USA, July 16-21.

Sterbentz, J.W., Hawkes, G.L., Maki, J.T., Petti, D.A., 2010. Monte Carlo Depletion Calculation for the AGR-1 TRISO Particle Irradiation Test. Transactions of the American Nuclear Society, 102, 495-496.

Sterbentz, J.W., Harp, J.M., Demkowicz, P.A., Hawkes, G.L., Chang, G.S., 2015. Validation of the Physics Analysis used to Characterize the AGR-1 TRISO Fuel Irradiation Test. Proceedings of the ICAPP 2015 Conference, Nice, France, May 3-6.

Sterbentz, J.W., 2015. JMOCUP As-Run Daily physics Depletion Calculation for the AGR-3/4 TRISO Particle Experiment in ATR Northeast Flux Trap. ECAR 2753, Idaho National Laboratory (INL).

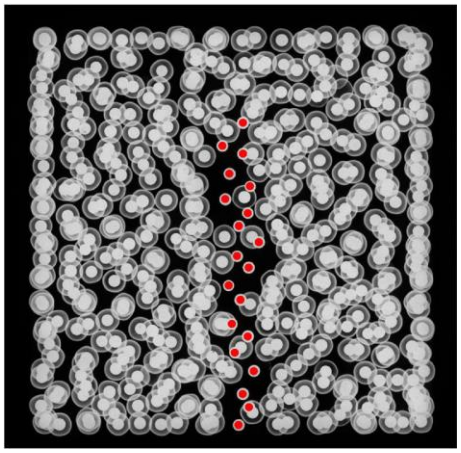

Figure 1. X-ray radiograph of a 2.5-mm thick section taken from the center of an AGR-3/4 compact showing the location (highlighted in red) of the 20 DTF particles (Hunn et al., 2014). The remaining particles are normal TRISO-coated driver particles.

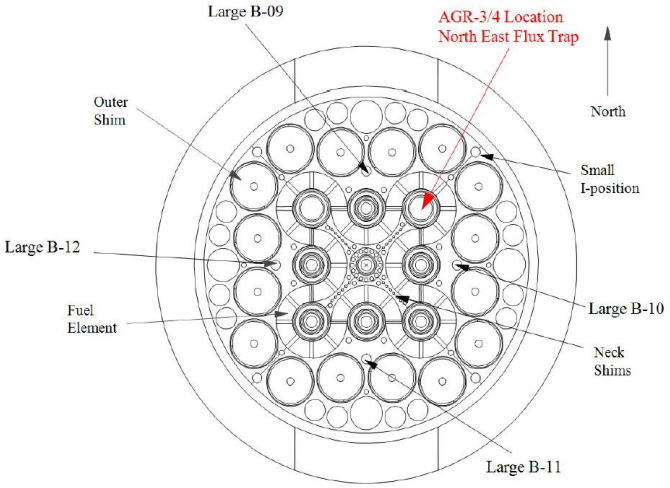

Figure 2. ATR core cross section displaying the northeast flux trap position.

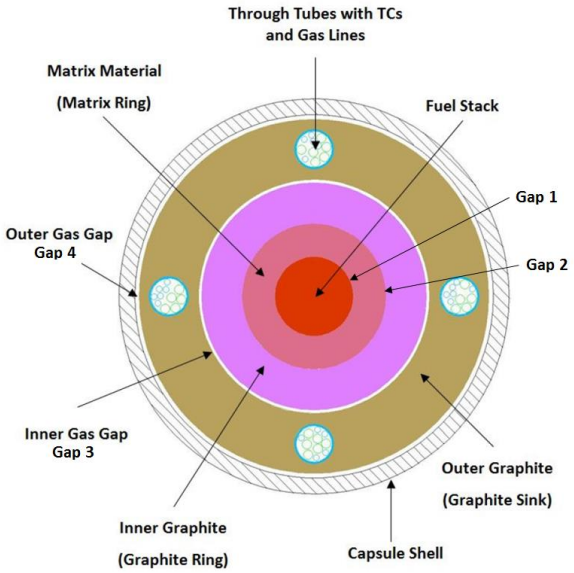

Figure 3. Radial schematic of an AGR-3/4 capsule.

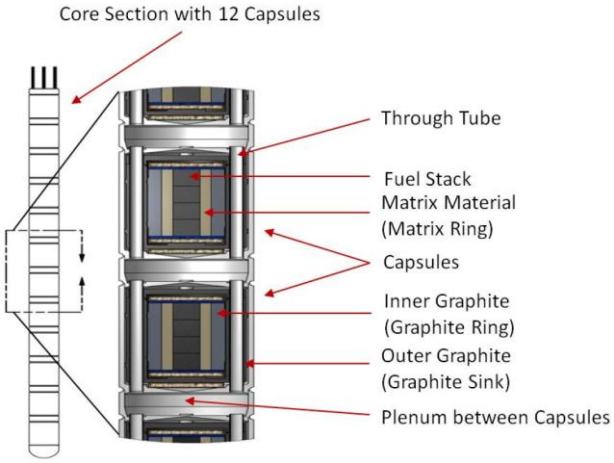

Figure 4. Axial schematic of the AGR-3/4 capsules.

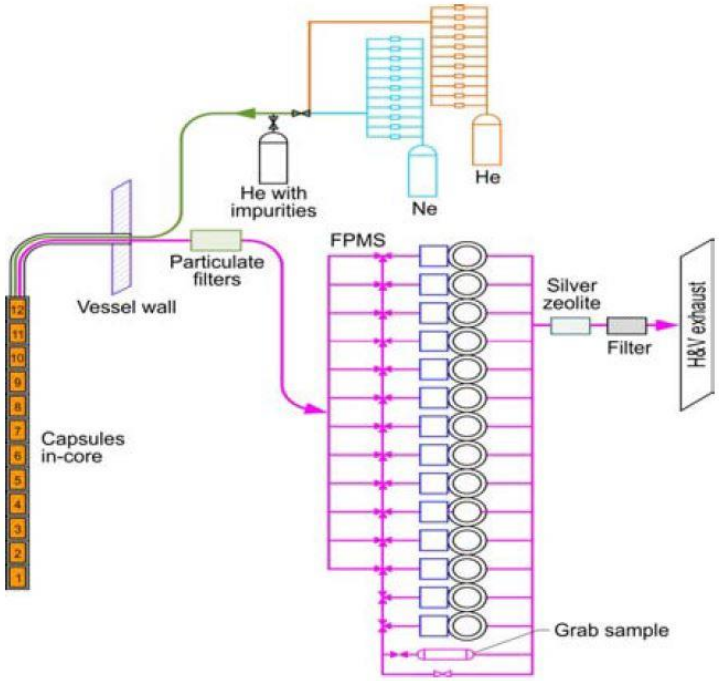

Figure 5. Flow path for AGR-3/4 sweep gas and Fission Product Monitoring System.

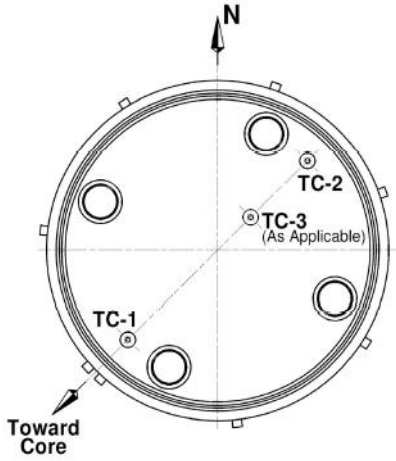

Figure 6. Cutaway view of an AGR-3/4 capsule showing the position of the thermocouples.

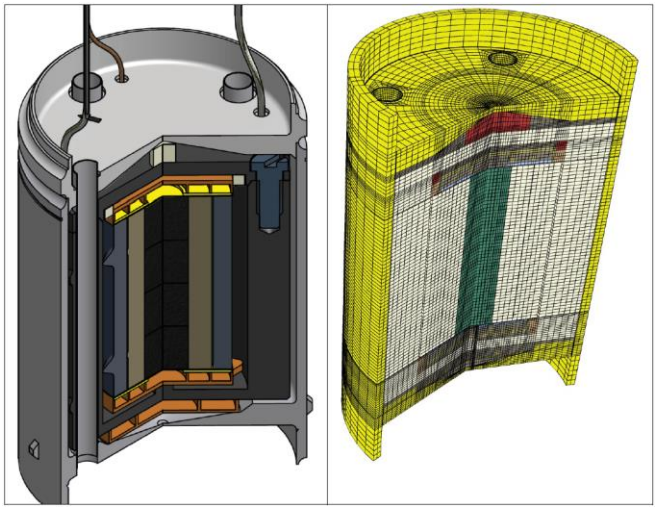

Figure 7. Cut-away view of an AGR-3/4 capsule and corresponding finite element mesh.

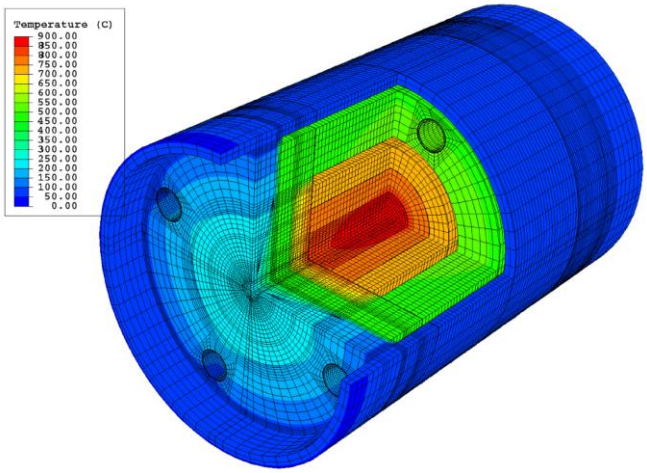

Figure 8. Cut-away view of a typical temperature (°C) contour plot of Capsule 12.

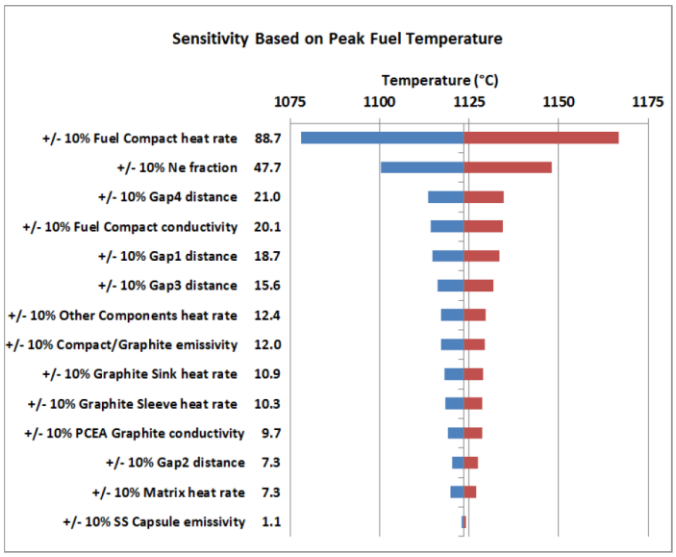

Figure 9. Tornado plot of peak fuel temperature sensitivity in Capsule 5 at one time step during the irradiation. The numbers to the left show the total temperature sensitivity.

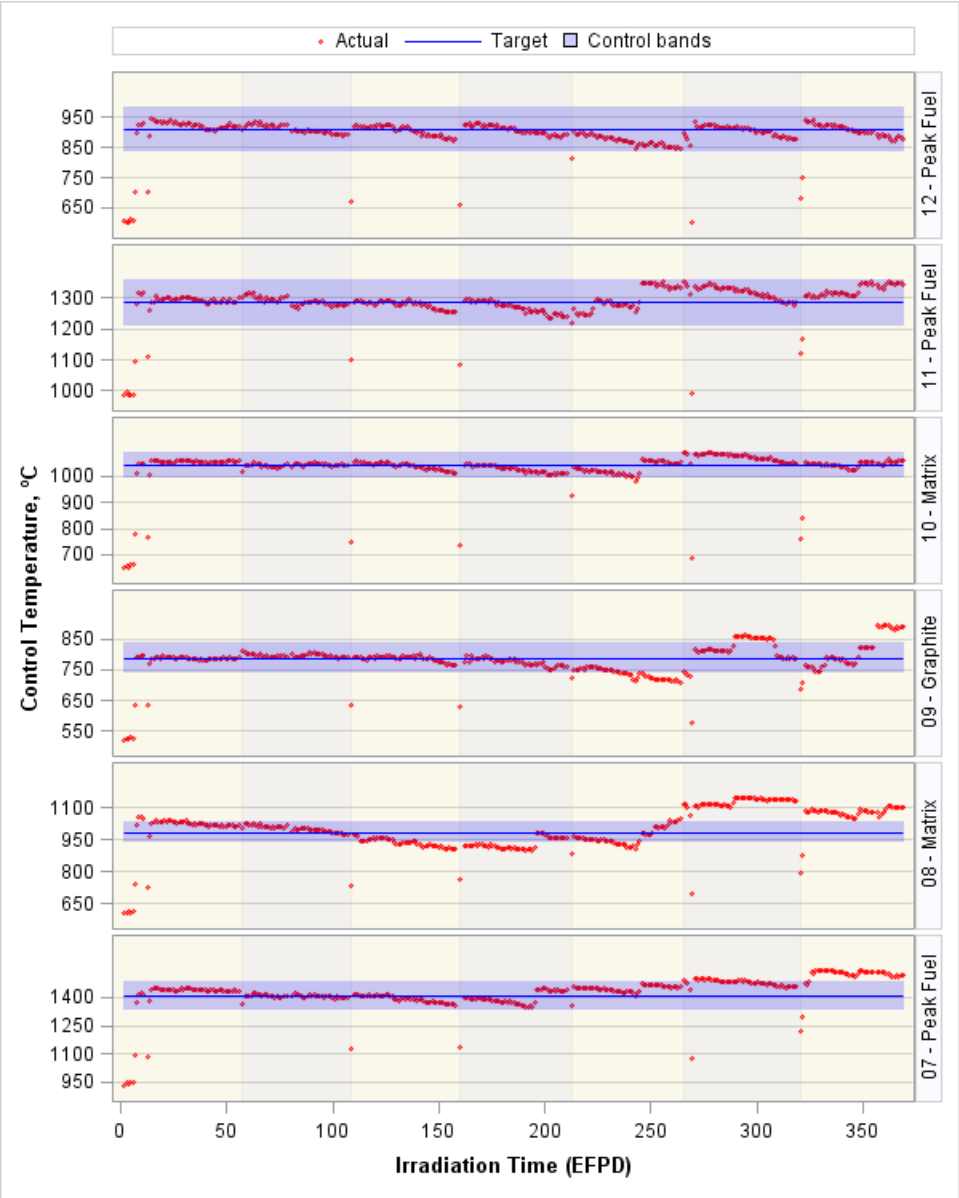

Figure 10. Calculated daily control temperatures for Capsules 7-12.

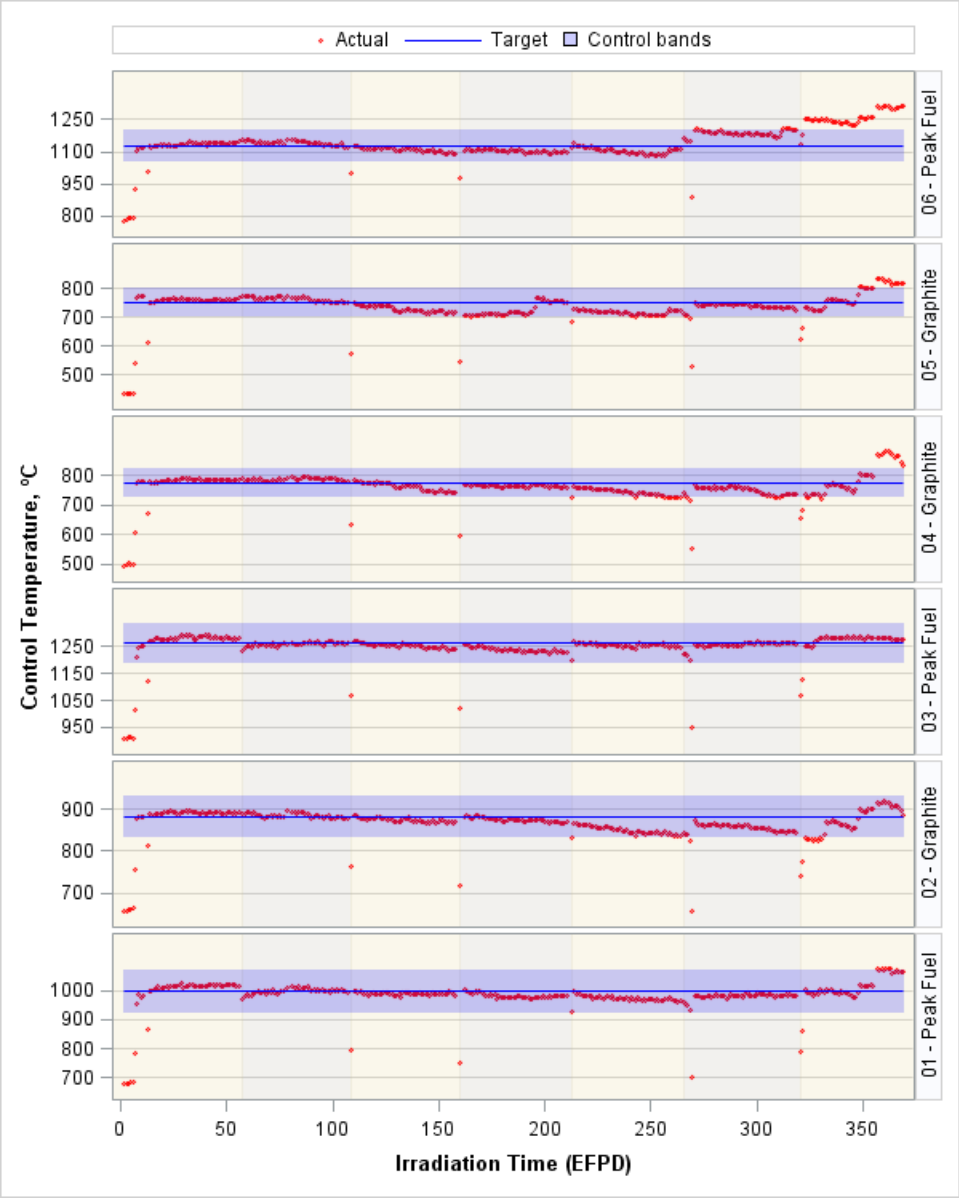

Figure 11. Calculated daily control temperatures for Capsules 1-6.

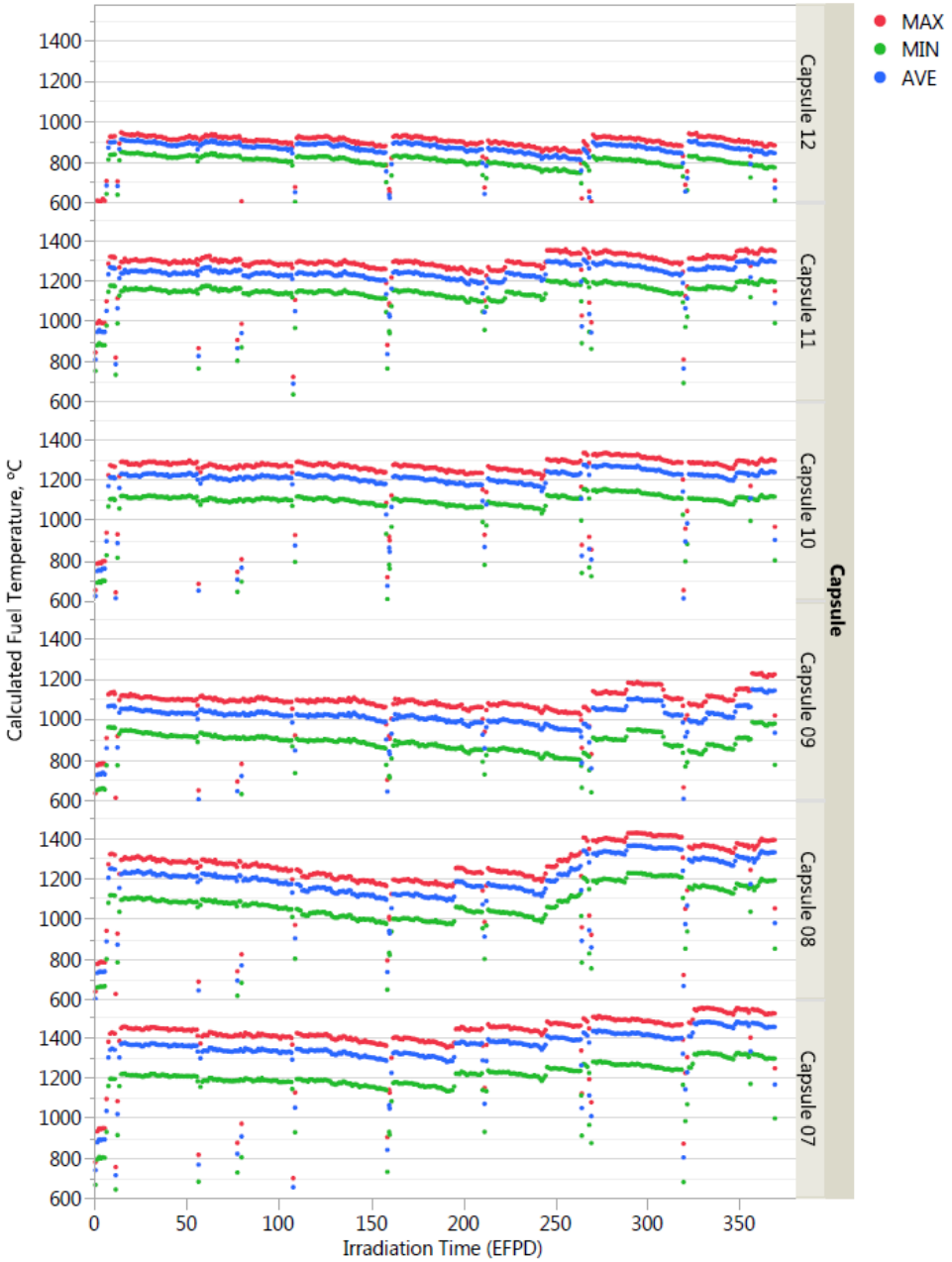

Figure 12. Calculated daily minimum, maximum, and volume-average fuel temperatures for Capsules 7-12.

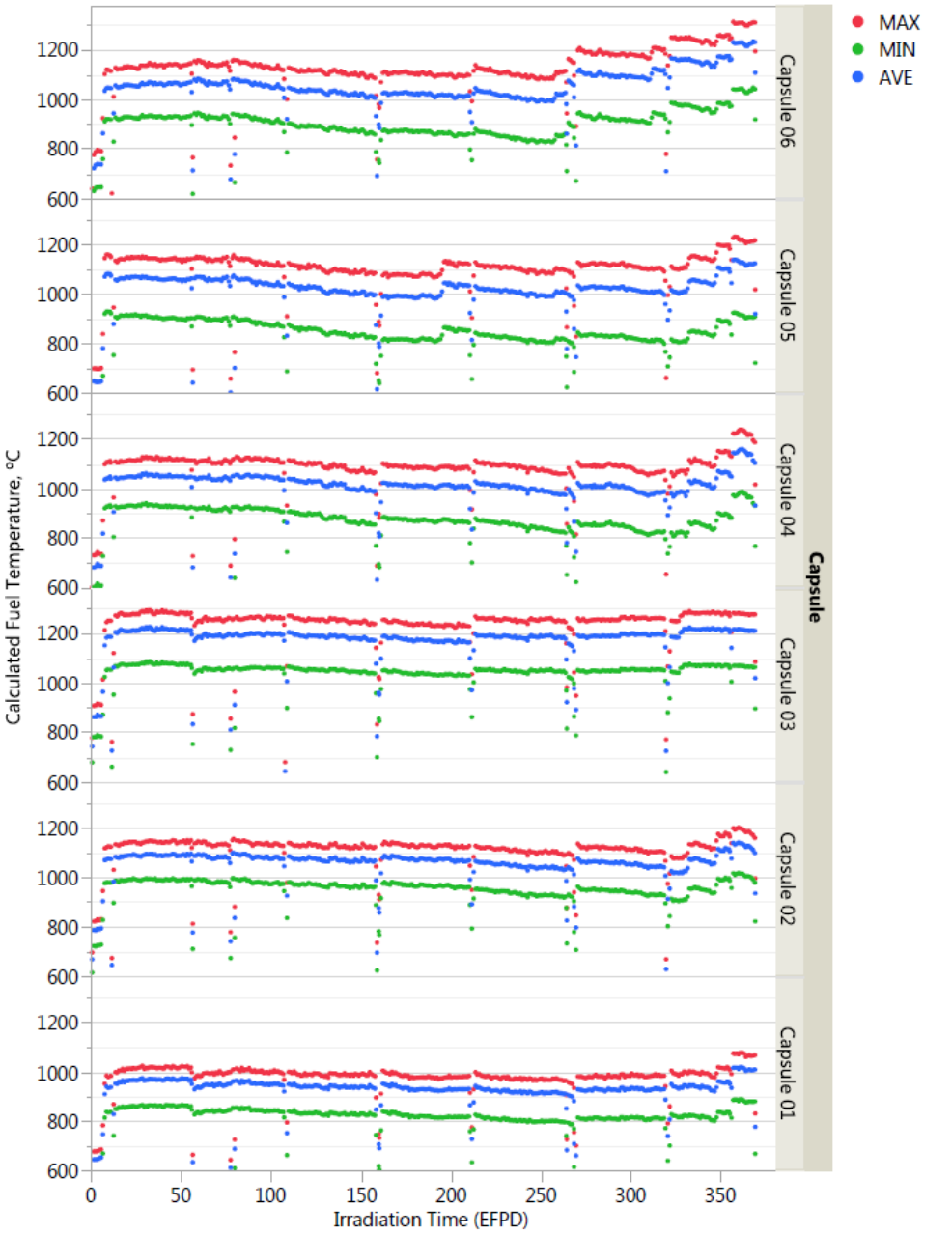

Figure 13. Calculated daily minimum, maximum, and volume-average fuel temperatures for Capsules 1-6.

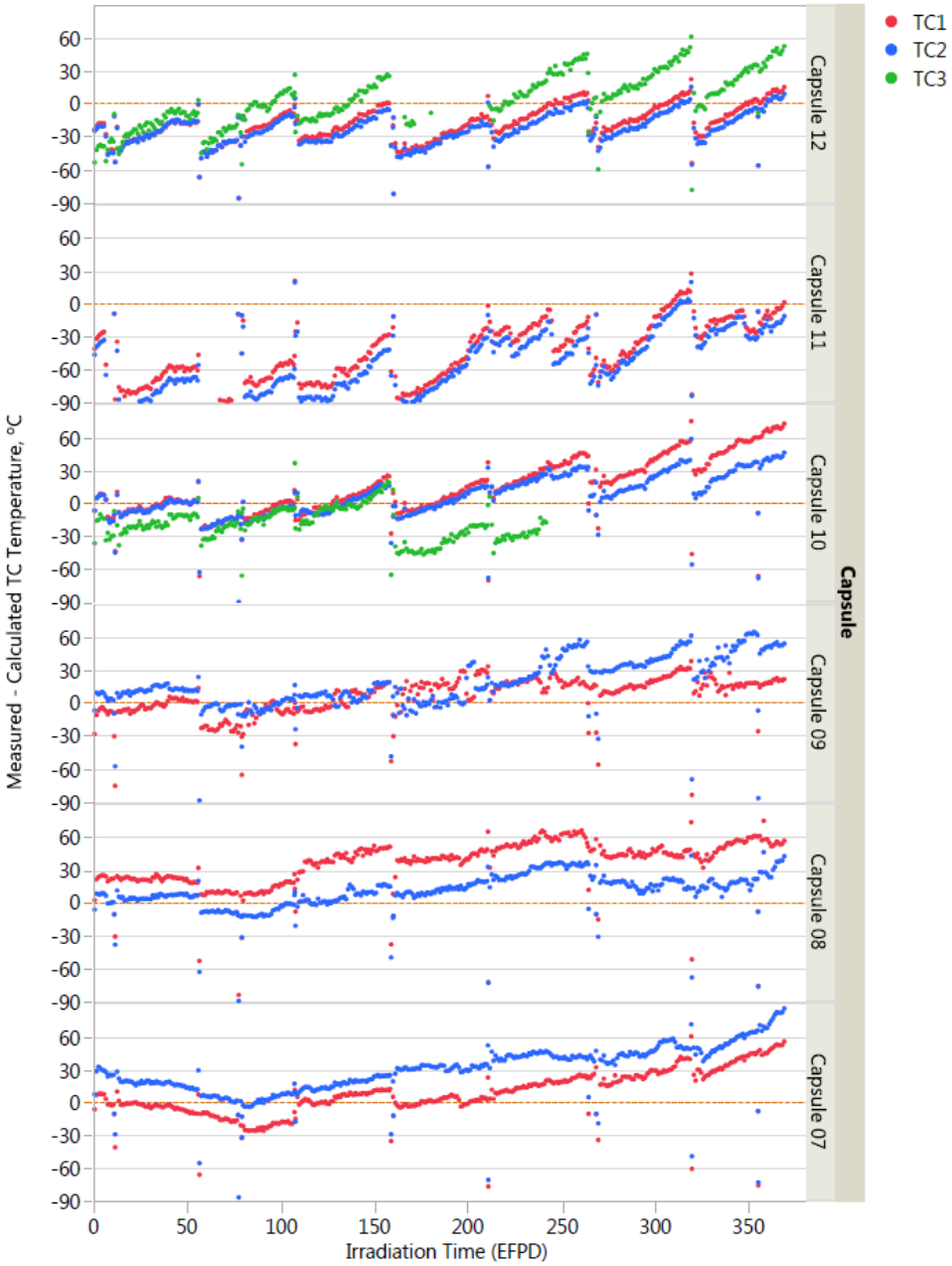

Figure 14. Difference between measured and calculated thermocouple temperatures versus irradiation time for Capsules 7-12. Note that some of the data sets terminate prior to the end of the irradiation due to TC failure.

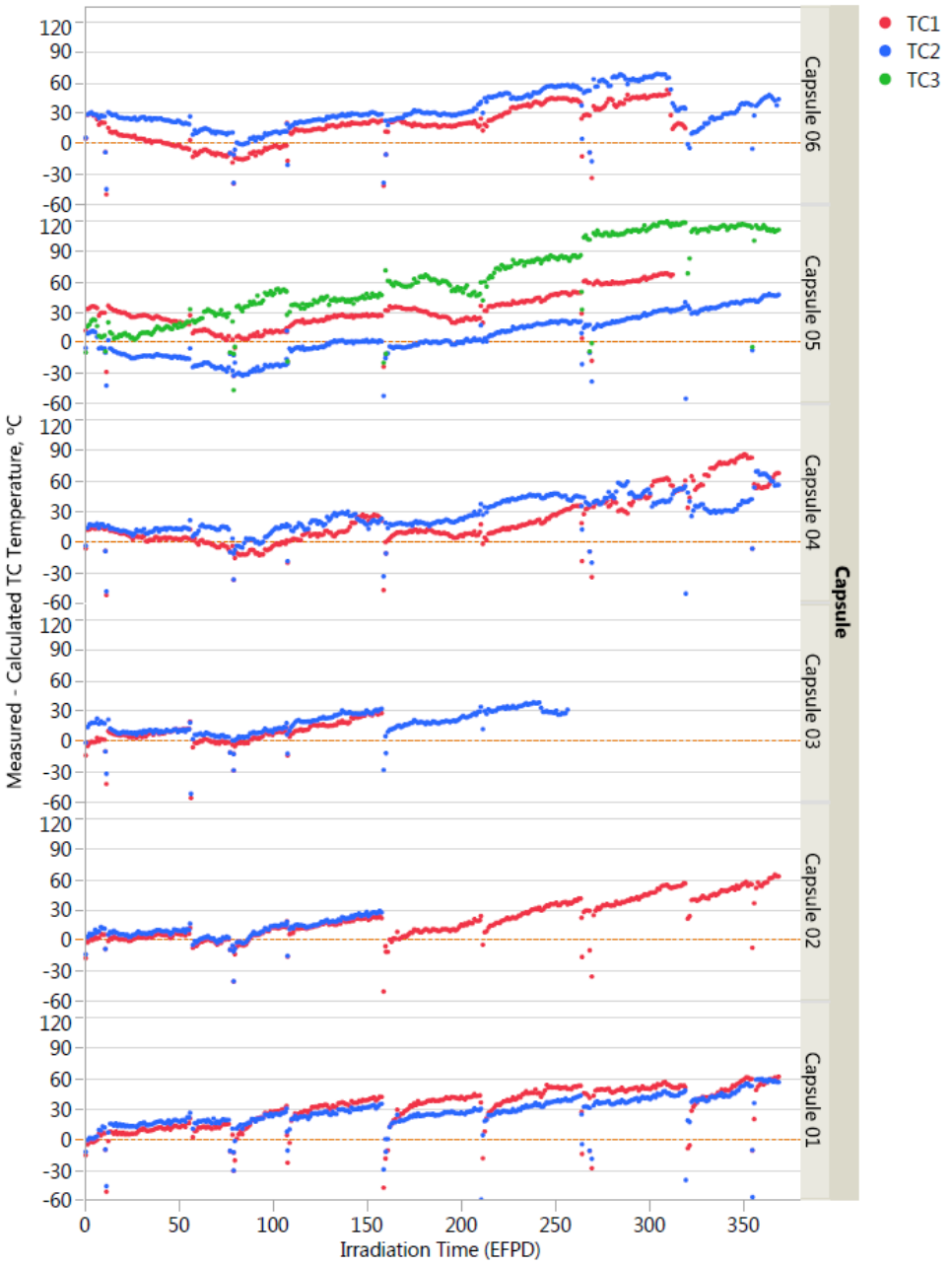

Figure 15. Difference between measured and calculated thermocouple temperatures versus irradiation time for Capsules 1-6. Note that some of the data sets terminate prior to the end of the irradiation due to TC failure.

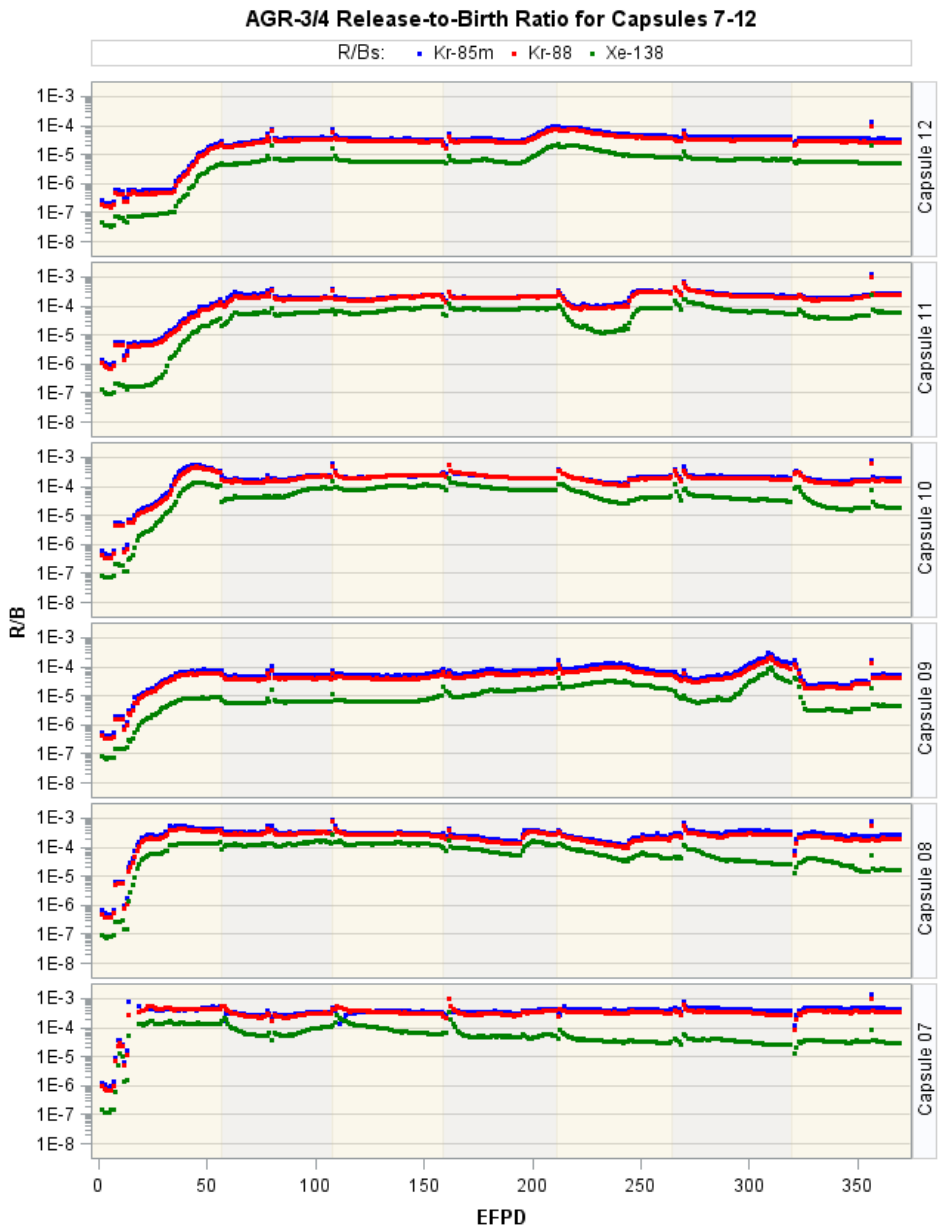

Figure 16. R/B ratios from daily birthrates for Kr-85m, Kr-88, and Xe-138 for Capsules 7-12.

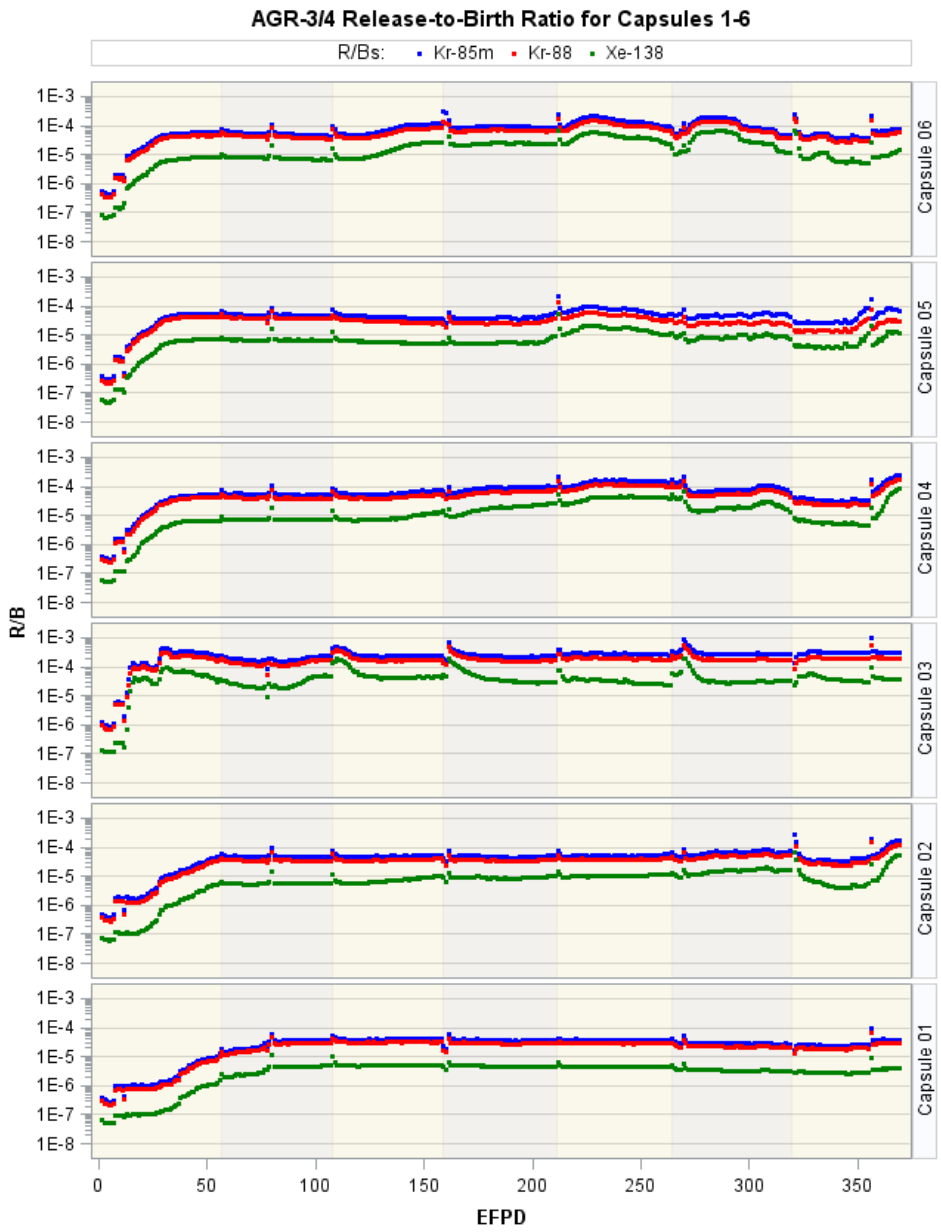

Figure 17. R/B ratios from daily birthrates for Kr-85m, Kr-88, and Xe-138 for Capsules 1-6.

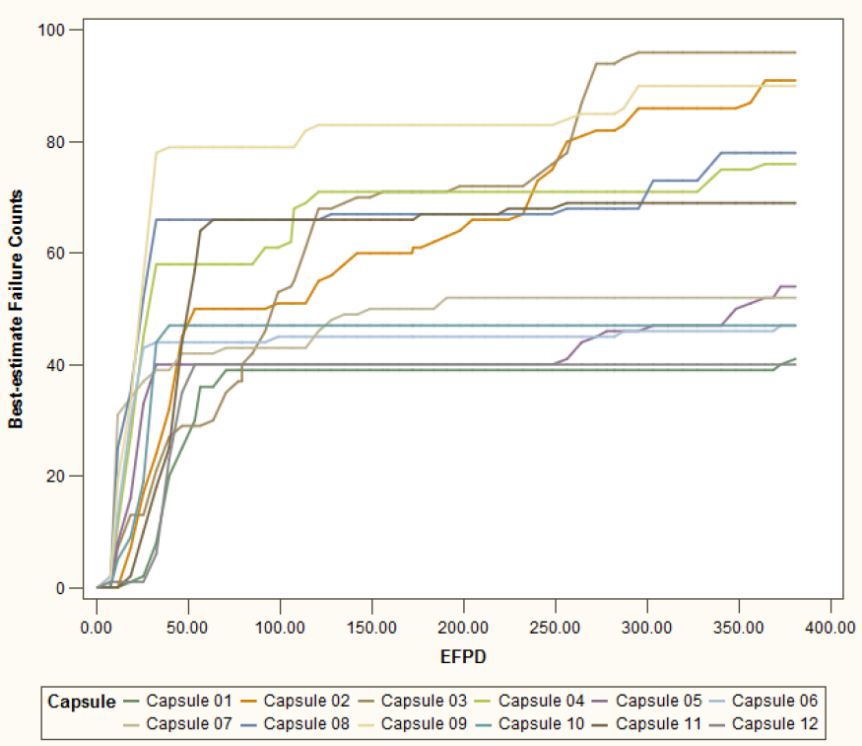

Figure 18. DTF best-estimate failure counts.

Table 1. Characteristics of the AGR-3/4 TRISO fuel particles and compacts.

Property	Mean Value ± Standard Deviation
Kernel properties	
Kernel diameter (μm)	357.3 ± 10.5
Kernel density (Mg/m^3)	11.098 ± 0.025
U-235 enrichment (wt%)	19.717 ± 0.014
Carbon/uranium (atomic ratio)	0.361 ± 0.004
Oxygen/uranium (atomic ratio)	1.43 ± 0.00
Driver fuel coating properties	
Buffer thickness (μm)	109.7 ± 7.7
Buffer density (Mg/m^3)	1.10 ± 0.04
IPyC thickness (μm)	40.4 ± 2.3
IPyC density (Mg/m^3)	1.904 ± 0.014
SiC thickness (μm)	33.5 ± 1.1
SiC density (Mg/m^3)	3.203 ± 0.002
OPyC thickness (μm)	41.3 ± 2.1
OPyC density (Mg/m^3)	1.901 ± 0.012
DTF fuel coating properties	
PyC seal coating thickness (μm)	20.0 ± 0.9
PyC seal coating density (Mg/m^3)	1.988 ± 0.009
PyC seal coating anisotropy	1.243 ± 0.019
Compact properties	
Compact diameter (mm)	12.310 ± 0.017
Compact length (mm)	12.510 ± 0.025
Compact matrix density (Mg/m^3)	1.603 ± 0.010
Number of driver particles per compact	1872
Number of DTF particles per compact	20
Particle volume packing fraction (%)	37
Effective overall compact density (Mg/m^3)	2.01

Table 2. AGR-3/4 graphite materials.

Capsule	Matrix Ring	Graphite Ring	Graphite Sink
12	ARB-B1[(a)]	PCEA	PCEA
11	ARB-B1	PCEA	PCEA
10[(b)]	PCEA	PCEA	PCEA
9	ARB-B1	IG-110	IG-110
8[(b)]	IG-110	IG-110	IG-110
7	ARB-B1	PCEA	PCEA
6	ARB-B1	PCEA	PCEA
5	ARB-B1	PCEA	PCEA
4	ARB-B1	PCEA	PCEA
3[(b)]	PCEA	PCEA	PCEA
2	ARB-B1	PCEA	PCEA
1	ARB-B1	PCEA	PCEA

(a) ARB-B1 is the name given to the fabricated lot of ring blanks used in the AGR-3/4 experiment. These ring blanks were made using a graphite/resin blend of natural and synthetic graphite flake mixed with a novolac resin (Hunn et al., 2011).
(b) Matrix material in the matrix rings of Capsules 3, 8, and 10 was replaced by fuel-element graphite to benefit from graphite at higher temperature.

Table 3. AGR-3/4 temperature matrix.

Capsule	Peak Fuel Temperature (°C)[(a,b)]	Matrix Ring Temperature (°C)[(a,b,c)]	Graphite Ring Temperature (°C)[(a,b,c)]	Initial Sink Temperature (°C)[(c,d)]
12	**900**	825-830	800-810	675-635
11	**1100**	985-1000	830-845	680-700
10	1130-1105	**980**	920-930	665-650
9	1080-1010	880-865	**800**	640-650
8	1180-1110	**980**	895-905	590-600
7	**1300**	1080-1175	1020-1115	585-690
6	**1100**	880-940	790-870	610-700
5	1040-960	830-810	**750**	580-570
4	1100-1050	890-870	**800**	610-630
3	**1250**	1080-1100	1025-1050	690-700
2	1050-1020	910-890	**850**	660-670
1	**950**	885	825	680

(a) Fuel temperature was controlled in Capsules 1, 3, 6, 7, 11 and 12 whereas graphite temperature was controlled in Capsules 2, 4, 5, 8, 9 and 10. Bold values are temperature specifications, other values result from calculations.
(b) When temperature ranges are shown, the first number is the estimated temperature at the beginning of the irradiation and second number is the estimated temperature at the end of the experiment.
(c) Temperatures at ring mid-point.
(d) The initial sink temperature is an acceptable range of temperatures for the mid-point of the sink ring at the beginning of irradiation.

Table 4. Uncertainties of the most significant parameters used in compact temperature calculation sensitivity study.

Parameter	Uncertainty (%)
Gap 1 width	10 – 40
Gap 3 width	1 – 50
Gap 4 width	1 – 10
Fuel compact heat rate	5
Neon fraction	3 – 5
Fuel compact conductivity	20

Table 5. Minimum, capsule-average, and peak compact burnup (%FIMA) at the end of irradiation.

Capsule	Minimum Compact	Capsule Average	Peak Compact	Goals
12	4.85	5.35	5.87	
11	8.42	9.06	9.64	
10	11.43	11.80	12.08	Minimum > 6%[(a)] for all compacts
9	13.40	13.67	13.87	
8	14.43	14.51	14.58	
7	14.90	14.96	15.02	Maximum < 10%[(b)] for two capsules
6	15.21	15.24	15.27	
5	14.74	14.87	14.98	
4	13.98	14.21	14.41	Maximum < 19% for all capsules
3	12.16	12.58	12.93	
2	9.43	10.07	10.65	
1	5.43	6.14	6.85	

(a) 42 of 48 compacts exceeded an average burnup of 6%.
(b) Three capsules had a maximum fuel compact burnup < 10%.

Table 6. Minimum, capsule-average, and peak compact fast fluence (10^{25} n/m^2, E >0.18 MeV) at the end of irradiation.

Capsule	Minimum Compact	Capsule Average	Peak Compact	Goals
12	1.19	1.50	1.80	
11	2.61	2.87	3.11	
10	3.75	3.94	4.12	
9	4.53	4.65	4.76	Minimum > 1.0
8	5.02	5.08	5.13	
7	5.24	5.27	5.29	
6	5.30	5.31	5.32	
5	5.14	5.19	5.23	
4	4.74	4.85	4.92	Maximum < 5.5
3	4.04	4.22	4.38	
2	2.95	3.21	3.44	
1	1.42	1.76	2.10	

Table 7. Time-average (TA) minimum, capsule-average, and TA peak temperatures (°C) at the end of irradiation.

Capsule	TA Minimum	Capsule Average	TA Peak	Goals[a]
12	790	854	888	
11	1134	1226	1280	
10	1079	1191	1249	TA peak = 900 ± 50°C for one capsule
9	875	1008	1083	
8	1063	1190	1257	TA peak = 1100 ± 50°C for up to six capsules
7	1197	1345	1418	
6	896	1051	1133	TA peak = 1200 ± 50°C for up to four capsules
5	838	1015	1102	
4	867	1008	1084	TA peak = 1300 ± 50°C for one capsule
3	1041	1177	1242	
2	951	1057	1113	
1	817	927	978	

(a) Two capsules had peak temperatures in the 1300 ± 50°C range and two capsules (Capsules 1 and 7) had peak temperatures that did not fall into any specified range.

Table 8. AGR-3/4 DTF fuel failure count.

Capsule	Minimum	Best-estimate	Maximum
12	38	39	49
11	48	69	92
10	36	47	75
9	88	90	99
8	54	78	129
7	38	52	75
6	42	47	53
5	36	54	92
4	57	76	100
3	53	96	164
2	51	91	168
1	21	41	81